Computational Analysis of Aza Analogues of [2′,5′-Bis-*O*-(*tert*-butyldimethylsilyl)-*β*-D-ribofuranose]-3′-spiro-5″-(4″-amino-1″,2″-oxathiole-2″,2″-dioxide) (TSAO) as HIV-1 Reverse Transcriptase Inhibitors: Relevance of Conformational Properties on the Inhibitory Activity

Elena Soriano,*,† José Marco-Contelles,‡ Cyrille Tomassi,§ Albert Nguyen Van Nhien,§ and Denis Postel§

Laboratorio de Resonancia Magnética, Instituto de Investigaciones Biomédicas (CSIC), C/ Arturo Duperier 4, 28029 Madrid, Spain, Laboratorio de Radicales Libres, IQOG (CSIC), C/ Juan de la Cierva 3, 28006 Madrid, Spain, and Laboratoire des Glucides (UMR 6219), Faculté des Sciences, Université de Picardie Jules Verne, 33 rue Saint Leu, 80039 Amiens, France

Received February 2, 2006

We have carried out a theoretical analysis of aza analogues of [2′,5′-bis-*O*-(*tert*-butyldimethylsilyl)-*β*-D-ribofuranosyl]-3′-spiro-5″-(4″-amino-1″,2″-oxathiole-2″,2″-dioxide) by a variety of computational tools, aimed to account for the effect of the endocyclic amino moiety *N*-2″ on the inhibitory activity against HIV-1. Docking studies suggest that compounds substituted at the *N*-3 and *N*-2″ positions present the same binding mode to the [2′,5′-bis-*O*-(*tert*-butyldimethylsilyl)-*β*-D-ribofuranosyl]-3′-spiro-5″-(4″-amino-1″,2″-oxathiole-2″,2″-dioxide)thymine prototype, where the endocyclic amino group remains mostly exposed to the solvent. A careful conformational analysis performed through different theoretical levels, from molecular mechanics to high-level quantum mechanical calculations, provides a rationalization based on conformational preferences, which appears as strongly determined by the substitution at *N*-2″, and on electrostatic effects from the bulk water.

1. INTRODUCTION

Reverse transcription of the viral single-stranded RNA genome into double-stranded DNA is a fundamental step in the replication cycle of the human immunodeficiency virus (HIV). This process depends on the enzymatic activities of the retroviral enzyme reverse transcriptase (RT). HIV RT is a multifunctional enzyme exhibiting two main activities: (1) a DNA polymerase activity, which can use both RNA or DNA as a template, and (2) an endonucleolytic ribonuclease H (RNase H) activity, which degrades the RNA strand of RNA:DNA duplexes.

RT is a heterodimer containing two subunits: the p66 subunit (560 amino acids), which exhibits both DNA polymerase and RNase H activity, and the p55 subunit (440 amino acids), which presents a closed, compact, folded conformation that causes the active site residues to be buried and, therefore, nonfunctional[1,2] but simultaneously provides structural support to the polymerase domain of the open-active conformation of the p66 subunit.[3] However, both of the monomers are functionally inactive when dissociated from each other,[4] which suggests that a worthwhile antiretroviral strategy might be based on agents that could disrupt the dimerization process of HIV-1 RT.[5] Some studies have evaluated the ability of different non-nucleoside inhibitors (NNRTI) to impact on the dimeric structure of HIV-1 RT.[6−8]

The [2′,5′-bis-*O*-(*tert*-butyldimethylsilyl)-*β*-D-ribofuranosyl]-3′-spiro-5″-(4″-amino-1″,2″-oxathiole-2″,2″-dioxide)-thymine (TSAO-T; Figure 1) was first described in 1992 by Camarasa et al. as a specific anti-HIV agent.[9]

Despite that the TSAO compounds show some inhibition characteristics of non-nucleoside RT inhibitors, acting through a noncompetitive mechanism against the substrate and template/primer,[10] they represent a singular class of RT inhibitors. The peculiar emergence of a strain of HIV-1 resistant to the TSAO displaying a Glu → Lys mutation at position 138 in the p51 subunit of HIV-1 RT has been reported,[11,12] thus suggesting that TSAO may not bind to the usual and well-defined non-nucleoside inhibitor binding pocket of HIV-1 RT (placed close to but distinct from the polymerase-active site of p66) but, rather, may bind to a different region partially overlapping with this pocket which involves the Glu138 residue.[13] The Glu138 residue in p51 is located in the *β*7−*β*8 loop, which also contains five other residues (amino acids from 134 to 139, SINNET sequence), and is an important component of the p51/p66 dimer interface. The crystal structure of HIV-1 RT reveals that the *β*7−*β*8 loop of p51 fits into the groove-like region on the floor of the polymerase cleft of p66, and therefore, it likely stabilizes the polymerase domain of p66. It has been demonstrated that the p51 subunit is involved in loading the p66 subunit onto the template primer for DNA synthesis[3] and that the intact *β*7−*β*8 loop of the p51 subunit is essential for the polymerase function of the p66 subunit.[14] Therefore, the binding of TSAOs induces unique conformational perturbations in the p66/p51 interface, which results in a

* Corresponding author phone: 34 00 913987320; e-mail: esoriano@iib.uam.es.
† Instituto de Investigaciones Biomédicas (CSIC).
‡ Laboratorio de Radicales Libres, IQOG (CSIC).
§ Université de Picardie Jules Verne.

10.1021/ci0600410 CCC: $33.50 © 2006 American Chemical Society
Published on Web 05/12/2006

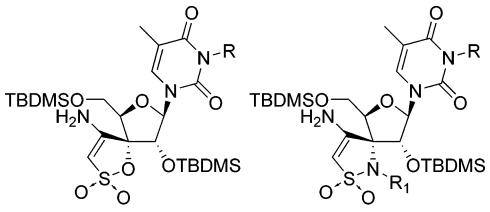

1: R= H, (**TSAO-T**)
2: R= CH_3, (**TSAO-m^{3}T**)

aza-TSAO derivatives
3: R= H, R_1= H
4: R= Boc, R_1= H
5: R= CH_3, R_1= H
6: R= C_2H_5, R_1= CH_3
7: R= H, R_1= CH_3
8: R= CH_3, R_1= CH_3
9: R= Boc, R_1= CH_3

Figure 1. Structures of TSAO-T and aza-TSAO derivatives.

marked destabilization of the dimeric structure of the enzyme, leading to a loss in its ability to bind DNA.[15]

A previous detailed molecular modeling study by Gago et al.[16] has indicated that TSAO binds at the interface between the two subunits where the amino group of the crucial 3′-spiro group forms a hydrogen bond with the carboxylate of Glu138 of the p51 subunit, consistent with the observed resistance of HIV-1 to TSAO analogues to mutations of this residue,[11,12] while the sulfone oxygen atoms are accommodated within the positive electrostatic region formed by Lys101 and Lys103 in the p66 subunit. Moreover, a hydrogen bond was observed between the O4 of the thymine ring and the hydroxyl group of Thr139 in the p51 subunit. Additionally, side chains from residues present at the enzyme interface (Ile31, Val35, Lys32, and Ser134 in the p51 subunit and Pro176 and Val179 in the p66 subunit) provide hydrophobic binding pockets for the 2′- and 5′-*tert*-butyldimethylsilyl (-TBDMS) substituents.[16]

Because TSAOs are highly functionalized nucleosides, a wide range of modifications have been designated and analyzed to assess the structural requirements for their optimal interaction with HIV-1 RT. Thus, structure−activity relationship (SAR) studies have revealed that the *ribo* sugar plays an essential role in the interaction with the enzyme and that the simultaneous presence of a 3′-spiro-5″-(4″-amino-1″,2″-oxathiole-2″,2″-dioxide) moiety and TBDMS groups at both the 2′ and 5′ positions of the sugar moiety is a prerequisite for antiviral activity.[17] The introduction of several modifications on the groups at 2′ and 5′ positions,[18] on the 3′-spiro moiety,[19] as well as on the base part,[20] has been performed and evaluated. In this regard, the replacement of the endocyclic oxygen by a nitrogen on the 3′-spiro sulfone has also been investigated (aza-TSAO derivatives, Figure 1).[21] The evaluation of the inhibitory activity against HIV-1 RT of these aza-TSAO derivatives showed remarkable trends. Thus, those aza derivatives bearing a methyl-substituted nitrogen in the spiro group (R_1 = Me, Figure 1) were ∼10-fold less inhibitory than the unsubstituted derivatives (R_1 = H, Figure 1), which proved to be only 2- to 8-fold less active against HIV-1 replication than TSAO-T. Both aza-compound series were not inhibitory against HIV-2, in analogy with the TSAO-T prototype.[21]

The presence of an additional H-bond donor group (R_1 = H, Figure 1) may provide further interaction points with other residues in the enzyme, which could give rise to a somewhat different binding mode. On the other hand, lesser activity shown by the methyl derivative could be attributable to unfavorable effects arising from the methyl substituent. To shed light on the role played by the N-2″ group, herein, we report the computational study on these aza-TSAO derivatives.

2. COMPUTATIONAL METHODS

Molecular Docking. All docking studies were performed with the program AutoDock (version 3.0.5).[22] As protein targets, we selected two wild-type unliganded forms (apoenzymes; PDB codes 1DLO[23] and HMV[24]) and five crystallographic structures of RT-NNRTI complexes (PDB codes 1BQM,[25] 1DTQ,[26] 1HNI,[27] 1S6P,[28] and 3HVT[29]). The water molecules, ions, and ligand structures were deleted, and polar hydrogens were added. Affinity grid files were generated using the auxiliary program AutoGrid (version 3.0). The carboxylic carbon atom of the residue GluB138 was chosen as the center of the grids, and the dimensions of the cubic grid were 90 × 90 × 90 Å^3 with grid points separated by 0.300 Å. At each grid point, the receptor's atomic affinity potentials for aliphatic carbon, aromatic carbon, oxygen, nitrogen, fluorine, chlorine, bromine, sulfur, and hydrogen atoms were computed for intra- and intermolecular energy evaluation of each docked configuration. The parameters not included by default in the docking program for computing the atom-specific affinity maps were incorporated.[30] For simplicity, the Si atoms were assimilated to aliphatic C atoms. The original Lennard-Jonnes and hydrogen-bonding potentials provided by the program were used. Amber united-atom charges and solvation parameters were assigned to the protein with the program ADT (AutoDock Tools, version 1.3a.1).

The ligand coordinates were obtained from ab initio geometry optimizations. Changes in ring puckering for the TSAO derivatives (**1**, **3**−**9**) were incorporated through consecutive docking analyses of different conformers (^{0}E, ^{2}E, and ^{3}E). These three conformers for each compound (**1**, **3**−**9**) and the NNRTIs used as controls in the docking experiments were fully optimized by means of the ab initio Hartree−Fock method and the 3-21G* basis set implemented in the quantum mechanical program Gaussian 98.[31] A common set of atom-centered RHF/6-31G*//RHF/3-21G* charges was then derived by using the restrained electrostatic potential methodology.[32]

The genetic algorithm implemented in AutoDock was used to generate different RT-bound ligand conformers by randomly changing the torsion angles and overall orientation of the molecule (see Table 1 in the Supporting Information for details). After docking, the 100 solutions were clustered in groups with root-mean-square (RMS) deviations less than 1.0 Å. The clusters were ranked by the lowest-energy representative of each cluster.

MIF Calculations. To prove the binding mode for the TSAO derivatives, molecular interaction fields (MIFs) were additionally calculated with the GRID methodology[33] on the target protein. MIFs identify regions on the enzyme where the functional groups present in the ligand can interact favorably, suggesting complementary positions. For the GRID calculations,[34] a 30 × 30 × 30 Å^3 lattice of points centered at the carboxylic carbon atom of the residue GluB138, and spaced at 0.250 Å, was selected. The probes

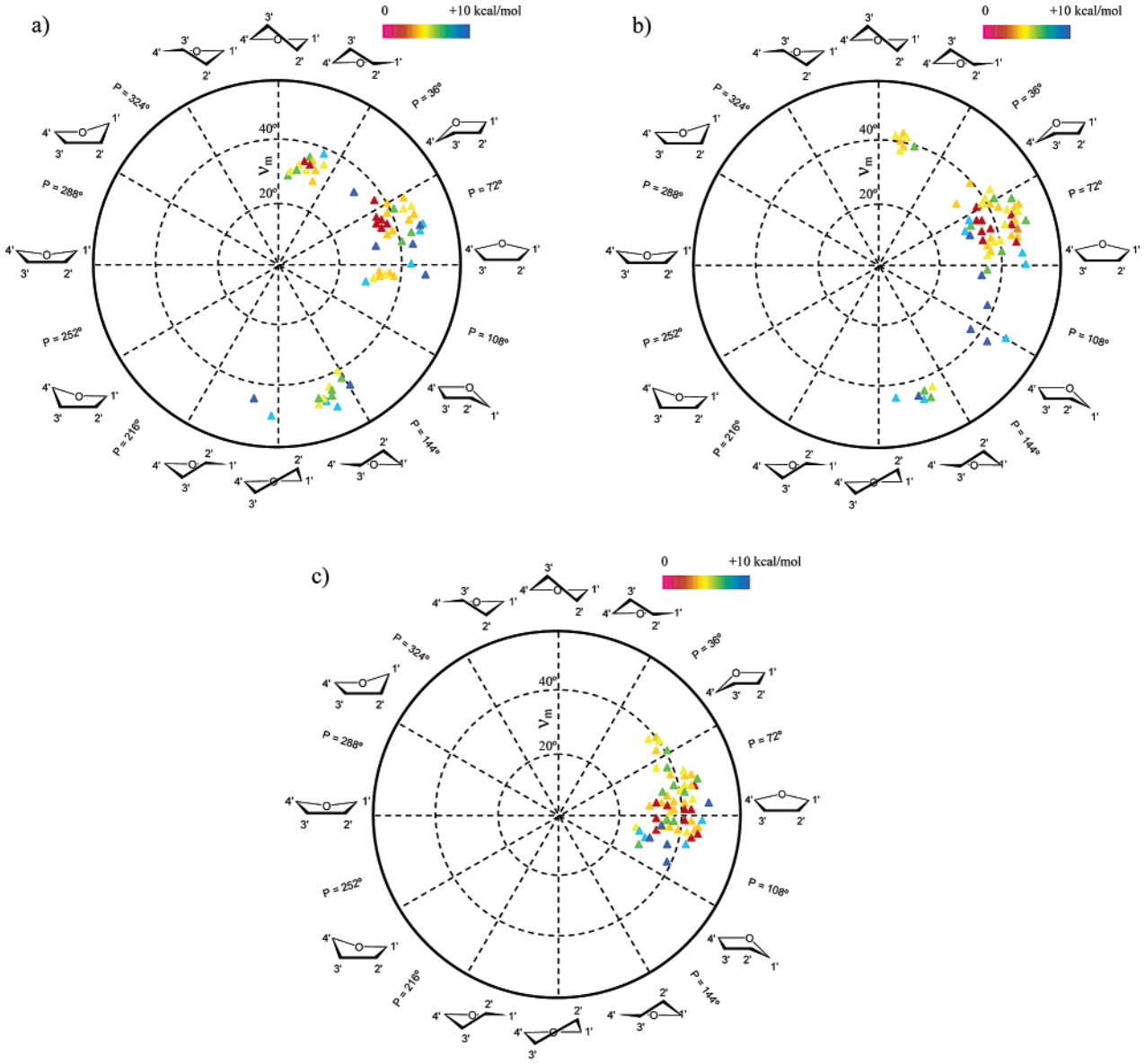

Figure 2. Pseudorotation cycle of the furanose ring. The preferred conformations as a function of P and ν_m for **10** (a), **11** (b), and **12** (c) are colored according to their relative energy.

used were N2 (neutral flat NH_2), O═S (oxygen of sulfones), and O (sp^2 carbonyl oxygen). The dielectric constants chosen were 4.0 for the macromolecule and 80.0 for the bulk water.

Conformational Search. Conformational analyses of compounds **1**, **10**−**12** were performed with PC SpartanPro[35] by means of the Monte Carlo algorithm[36] for the random variation of all of the rotatable bonds and the MMFF94 force field[37] as an energy minimization method. Endocyclic sugar atoms were allowed to be puckered up and down. Default values were set for the nonbonded interactions cutoff. For each search, about 1000 (2000 for **1**) starting structures were generated and minimized. Duplicated structures and those higher in energy than ~10 kcal/mol above the global minimum were discarded. Then, the pseudorotational phase angle P, as a function of the five endocyclic torsion angles ν_0, ν_1, ν_2, ν_3, and ν_4, and the puckering amplitude (ν_m) were calculated (see the Supporting Information for details) for each final structure and represented in graphical plots (Figure 2).

Ab Initio Conformational Energy Profiles. Ab initio molecular orbital calculations were performed with the Gaussian 98[31] and Gaussian 03[38] suites of programs. The seven envelope forms (^{3}E, $_4$E, ^{0}E, $_1$E, ^{2}E, $_3$E, and ^{4}E) of **10**−**12** were examined by holding one endocyclic torsion angle fixed in each of seven computations (i.e., for ^{0}E, the C1−C2−C3−C4 torsion was held constant at 0° and so forth).[39] All remaining structural parameters were allowed to relax in each calculation. This constrained geometric optimization was carried out at the Hartree−Fock level of theory, with the 3-21G* basis set. Then, a single-point energy calculation at the DFT level (B3LYP hybrid functional[40]) with the 6-31G* basis set was performed on the optimized geometries. Additionally, solvent effects in the aqueous phase ($\epsilon = 78.4$) were evaluated by the polarizable continuum model CPCM[41] as implemented in Gaussian 03, with the options for the solvation model selected by default.

DFT Calculations. Full geometry optimizations of the most relevant conformers were performed both in a low-dielectric medium ($\epsilon = 4.0$) and in an aqueous solution ($\epsilon = 78.4$) at the DFT (B3LYP hybrid functional) level, by using the 6-31G(d) basis set. On the optimized structures, single-point energy calculations were carried out via the

B3LYP/6-31+G(2d,p) model to obtain more accurate energies. Previous studies on related structures have demonstrated that B3LYP/6-31+G(2d,p)//B3LYP/6-31G(d) combination yields energy values quantitatively similar to those obtained from full geometry optimizations at the B3LYP/6-31+G(2d,p) level.[42] Solvent effects were evaluated with CPCM, which employs conductor rather than dielectric boundary conditions. The dielectric constant chosen was $\epsilon = 4.0$, which is the standard value used to model protein surroundings, and $\epsilon = 78.4$ was chosen for the aqueous phase. Final total energy values, obtained from single-point calculations, include both electrostatic and nonelectrostatic contributions.

3. RESULTS

3.1. Docking Studies. Many crystal structures of HIV-1 RT have been reported in recent years, including unliganded, complexed to DNA, and complexed to several NNRTIs. Unfortunately, any cocrystallization attempts of the enzyme with TSAO derivatives have been unsuccessful. Although the overall RT shapes are relatively similar among the complex crystal structures, there are subtle differences between them which require a careful selection to achieve reasonable docking results.[43] Visual inspection of the p51/p66 interface revealed that the putative binding site varies in the crystallographic structures, in such a way that some of them did not present a large enough cavity between Glu138 (in p51) and Lys101 and Lys103 (in p66) to accommodate the spiro ring moiety. Hence, we selected two apoenzyme structures (PDB codes 1DLO[23] and HMV[24]) and five crystallographic structures of RT-NNRTI complexes (PDB codes 1BQM,[25] 1DTQ,[26] 1HNI,[27] 1S6P,[28] and 3HVT[29]). A comparison based on the superposition of all Cα positions between the unligated HIV-1 RT 1DLO and 1HMV structures shows an RMS deviation of 1.06 Å, while the Cα positions in the region comprising within 20 Å of the carboxylic carbon of Glu-B138 gives an RMS deviation of only 0.68 Å. As expected, the complexed protein structures show larger RMS deviations from 1DLO, ranging from 1.4 to 1.8 Å for the whole macromolecule to 0.9−1.4 Å for the relevant reduced region.

To validate the docking protocol, NNRTIs were also docked with their corresponding crystallographic enzyme structures as the protein targets. The results reproduced the crystal RT/NNRTI complex in every simulation. The RMS deviation between the best docked structure, which was generally the structure with the lowest docking energy in the most populated cluster, and the crystal structure was in the range 0.7−1.1 Å for all of the inhibitors, except for α-APA R 95845 (protein target 1HNI, 2.2 Å).

Despite the wide variety of binding modes found by the automated docking program for the aza-TSAO derivatives in the investigated region, the simulations yielded a significant cluster with docked structures in the presumed binding site for the TSAO-T prototype.[16] Remarkably, the structures within this cluster showed interaction energy values within the lowest energy range. The best results were observed from both apo forms (up to 12 occurrences) and from the complexed 1BQM (up to 14 occurrences) and 1HNI protein structures as input (up to 21 occurrences), the latter providing the largest clusters for the putative binding site.

The selected docked structures, depicted in Figure 3, situate in the heterodimer interface where the 3′-spiro group forms polar interactions with both subunits: the 4″-amino substituent interacts with the negatively charged carboxylate of Glu-B138 at the same time that the sulfone oxygen atoms point to the positive electrostatic region formed by Lys-A101 and Lys-A103 residues. The O4 of the thymine ring forms an additional H bond with the hydroxyl group of Thr139 in the p51 subunit. Also, the model reveals stabilizing hydrophobic interactions between the methyl groups of the TBDMS group at C-5′ of the inhibitor and p51 subunit residues (side chains of IleB31, LysB32, SerB134, and Val35) and between the C-2′ TBDMS group with the hydrophobic cavity formed mainly by p66 subunit residues

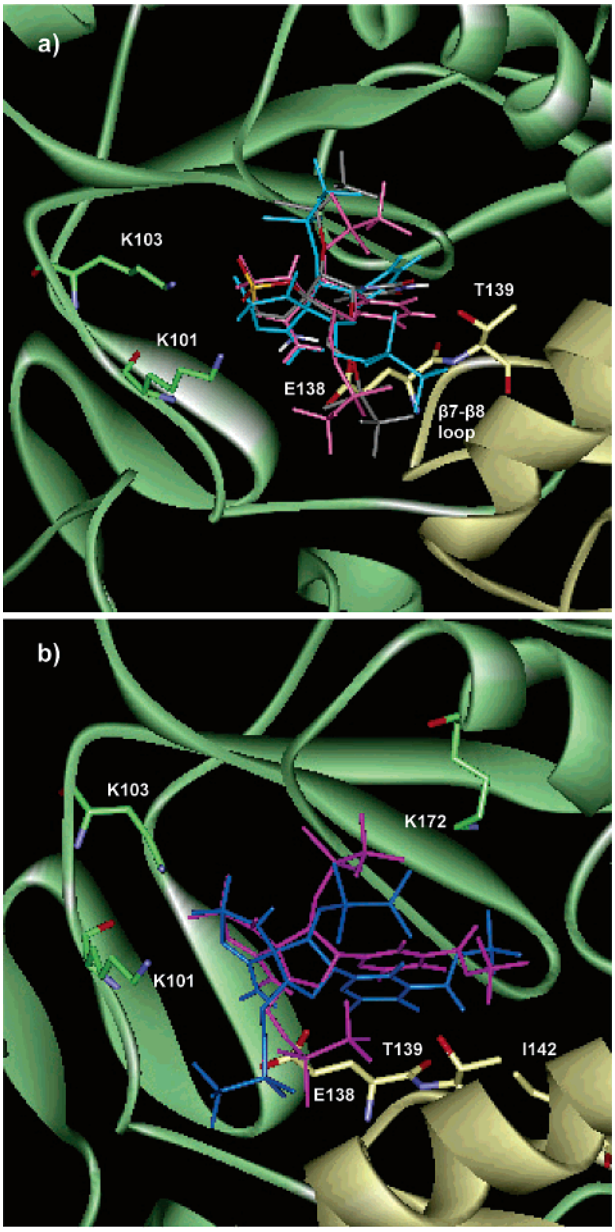

Figure 3. Binding model from docking simulations. The Cα trace of the enzyme is displayed as a ribbon, colored in green and yellow for the p66 and p51 subunits, respectively. The side chains of some relevant residues (LysA101, LysA103, LysA172, GluB138, ThrB139, and IleB142) are shown as thick sticks, with carbon atoms colored according to their subunit. TSAO inhibitors are displayed as thin sticks: (a) **3** (pink), **7** (blue), and **1** (colored by atom) for comparison; (b) *N*-3-substituted inhibitors **4** (deep blue) and **9** (magenta).

(side chains of ProA176, Val179, and LysA172).

The *N*-3 base substituent in **4**−**6**, **8**, and **9** rests parallel to the interface. As pointed out in a recent docking study, the introduction of functional groups at the *N*-3 position may induce further stabilizing interactions with the enzyme, thus giving rise to an increased activity.[20c] Our docking analysis for **4** (and **9**) suggests that the Boc moiety could establish additional hydrogen bonds with the enzyme, between the carboxylic oxygen of **4** (**9**) and the hydroxy group of the side chain of ThrB139 and the terminal amino group of the side chain of LysA172 (or ArgA172 in other HIV-1 strains; Figure 3b). On the other hand, further stabilization might be gained from van der Waals contacts with the side chain of IleB142. The reported inhibitory activities of **4** and **9** as compared with the unsubstituted structures **3** and **7** (0.43 and 3.5 μM vs 0.33 and 3.5 μM, respectively)[21] suggest that such interactions are probably weak or nonexistent. It could be argued that the bulkiness of the protecting group might obstruct an optimal interaction with ThrB139.

Overall, the docking study has revealed similar results for both series of aza derivatives. According to this binding mode, the endocyclic amino group in the 3′-spiro moiety would be mostly exposed to the solvent, thus making an almost negligible contribution to binding. The methyl substituent may involve steric hindrance with the C-2′ substituent, inducing a conformation with limited flexibility that could afford a less effective interaction with the enzyme. Therefore, differences in activity for both series can be attributed to subtle differences in scaffold geometry, and thus, a detailed conformational analysis is needed to assess the effect of the endocyclic amino group.

3.2. Calculation of MIFs. MIFs[33] computed with the GRID program[34] also confirmed the binding mode. The GRID procedure has been developed for determining energetically favorable binding sites for small chemical groups, called probes, on macromolecular targets. Thus, in the current study, we searched for sites in the protein that could more favorably interact with the functional groups in the inhibitor.[44] Because the 3′-spiro group may be placed in a cavity created by Lys-A101, Lys-A103, and Glu-B138, we selected N2 (neutral flat NH_2) and O═S (oxygen of sulfones) as probes for the GRID calculations. In addition, we included the O probe (sp^2 carbonyl oxygen) to check the interaction of O4 of the thymine ring with the hydroxyl group of ThrB139 and that, if any, of the substituent on *N*-3. The computed GRID isocontour energy maps plotted at an energy value of 70% of the corresponding best minimum GRID energy (Figure 4) highlight those regions in the target where the probe finds energetically favorable sites.[44] The maps show that the most (or one of the most) energetically favorable binding site for each probe situates in the expected position, and a good fit of overlaying maps graphically verifies the agreement with the docking results.

3.3. Conformational Study. It is well known that furanosyl rings can exhibit considerable conformational flexibility involving exchange between generalized North (N, $^3T_2$) and South (S, $^2T_3$) twisted conformers via a pseudorotational itinerary[45] or via inversion.[46] The substitution at the sugar ring carbons is expected to exert an important effect on the ring conformation, leading to preferred conformations depending on both the number and nature of the substituents.

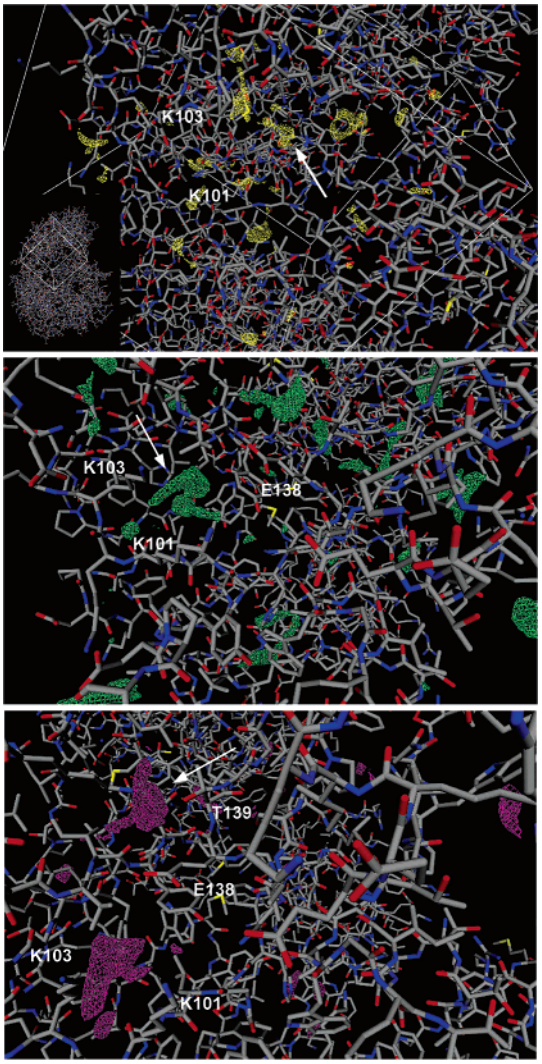

Figure 4. GRID isocontour maps generated by the amine N2 (yellow), sulfone oxygen O═S (green), and carbonyl oxygen O (pink) probes. The MIF fields, representing the energetically favorable regions, were generated at specific energy values corresponding to 70% of the minimum energy.

The overall conformation of a nucleoside can be described by the following structural parameters: (i) the glycosyl torsion angle (χ) about the *N*-glycosidic bond (N−C1′) that links the base to the sugar, (ii) the backbone torsion (γ), which determines the conformation about the C4′−C5′ bond, and (iii) the phase angle of pseudorotation (*P*), which effectively defines the sugar conformation on the basis of a wavelike motion from a chosen mean plane defined by five ring atoms, and the puckering amplitude (ν_m), which measures the extent of deviation of the ring torsion angles from planarity.[47]

In this report, we have investigated the conformational behavior of the oxo and aza derivatives by means of different theoretical methods. To save computational efforts, we have selected the structures **10**−**12**, shown in Figure 5, as theoretical models. First, a conformational search has been performed via molecular mechanics calculations (MMFF94 force field). Then, a constrained ab initio analysis of the pseudorotation itinerary as a function of the glycosyl and the C4′−C5′ backbone torsion angles has provided a clearer picture of the conformational energy profile. Finally, a DFT unrestricted optimization of geometry on crucial conformers

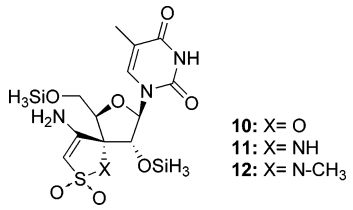

Figure 5. Structures of compounds **10**−**12**.

has been computed to determine the theoretically preferred conformation for every TSAO derivative. These results may provide insights into the conformational changes required to bind the enzyme and whether conformational differences could account for the variation observed in the inhibitory activity against HIV-1 RT.

3.3.1. Conformational Search. The results provided by the conformational searches using the MMFF94 force field are depicted in the Figure 2 for the three reduced models. For **10**, three main puckering modes for the sugar ring were clearly observed (Figure 2a), in the increasing energy order O4′-*endo* (^{0}E), C2′-*endo* (^{2}E), and C3′-*endo* (^{3}E). On the other hand, both syn and anti orientations of the thymine base relative to the ribose were found. The backbone torsion around the C4′−C5′ exocyclic bond gives rise to the three expected conformations, +*sc*, *ap*, and −*sc*.

It should be noted that, when this analysis was carried out on the full structures (for TSAO-T prototype, **1**, see Figure 2 in the Supporting Information), similar trends were observed, despite that they involved narrower *P* ranges. On the contrary, the puckering amplitude (ν_m) appeared less influenced, showing similar values (30−50°). Thus, for instance, while *P* varied in the ranges 7−25°, 45−100°, and 150−190° for the reduced model, **1** showed variations between 10 and 21°, 60 and 92°, and 158 and 180°. This effect is attributable to the TBDMS moieties, which may induce stronger steric interactions, limiting the ring flexibility to more restricted and defined regions of the pseudorotation circuit.

The conformations showing the lower energy values involve intramolecular hydrogen bonds between the spiro amino group and (a) the base O4 atom, stabilizing the syn conformations and the O4′-*endo* and C3′-*endo* puckering modes, and (b) O5′, increasing the stability the C2′-*endo* envelope form for the anti conformers. These results agree with the results from NMR studies, X-ray analyses, and molecular dynamics (MD) simulations reported for the TSAO-T and TSAO-m^{3}T structures.[15,16,48]

The analysis of the *N*-unsubstituted aza derivative **11** reveals strong similarities, although there is a more populated cluster in the East region of the pseudorotational cycle (Figure 2b). Syn and anti conformations are likewise observed, where both kinds of intramolecular H bonds stabilize the ^{0}E, ^{2}E, and ^{3}E envelope forms. Interestingly, the endocyclic amino group forms an additional H bond with the O2′ atom, which may somewhat restrict the puckering of the sugar ring. In sharp contrast, the methyl-amino derivative **12** yields a rather different conformational picture (Figure 2c). The most frequent and lowest-energy conformations involve *P* values within the restricted range 80−115°, showing a rather planar N environment (∼15°). While the unsubstituted aza-derivative conformers (**11**) present a highly pyramidalized endocyclic amino group, probably enhanced by the intramolecular H bond, the steric interactions between the methyl moiety and the sugar substituents for **12** induce limited conformations where the C1′−C2′−C3′−C4′ torsion angle (ν_2) appears close to zero.

Although this analysis may provide an overview of the conformational properties, in principle in agreement with experimental evidences, a more rigorous study is required to acquire accurate energy values. In addition, the observed high probability of intramolecular H-bond formation might be due to the parametrization procedure of this force field, on the basis of crystallographic data, which tends to overestimate them.

Our docking simulations and a previous molecular dynamics study[16] have suggested that the inhibitor would form no intramolecular H bonds upon binding with the enzyme. Moreover, the electrostatic effects of a polar solvent may disrupt the intramolecular H bond between the solvent-exposed endocyclic NH group and O2′ (for **11**). Therefore, a careful evaluation of the conformational energy profile in the gas and aqueous phases may shed light on the energy penalty involved in the expected conformational change on passing from the aqueous solution to the constrained complex form.

3.3.2. Ab Initio Conformational Energy Profiles. Theoretically, the pseudorotation angle (*P*) of the sugar ring of a nucleoside can vary between 0 and 360° but is usually limited to the physiological subrange from 20 to 200°. Therefore, we focused on the *P* range 18−234°, enclosing the envelope forms ^{3}E, E$_4$, ^{0}E, E$_1$, ^{2}E, E$_3$, and ^{4}E. We examined the conformational energy of **10**−**12** as a function of the pseudorotation phase angle, by holding one endocyclic torsion angle constant at 0° (see Computational Methods), in the three staggered C4′−C5′ rotamers (+*sc*, *ap*, and −*sc*) and with both thymine orientations (syn and anti). The energy profiles obtained are shown in Figures 6 and 7. The high degree of functionalization of the sugar ring gives rise to complex conformational energy profiles, where the structural and thermodynamic parameters are determined by van der Waals interactions, electrostatic interactions, and hydrogen bonding, while the anomeric effect is marginal.[49]

The analysis for **10** (Figure 6) reveals that the spiro amino group hydrogen-bonds to O5′ for the +*sc* rotamers, with the minimum energy structure at the ^{0}E and ^{2}E envelope forms. It is interesting to note that, despite the syn conformers providing a second H-bond acceptor group, the simultaneous formation of H bonds between −NH$_2$ and O5′ and O4 of thymine involves strong 1,3-diaxial interactions, which may account for the unexpectedly high energy of the C3′-*endo* (^{3}E) form relative to that of the anti rotamers.

The *ap* rotamers show intramolecular H bonds only for the syn orientation (−NH$_2$···O4), except for the ^{3}E endo form. For the anti orientation, a backbone torsion around the C2′−O2′ bond is observed during optimizations for $P \geq 90°$, to minimize the repulsive interactions with the endocyclic spiro oxygen (dihedral angle C1′−C2′−O2′−Si = −175° for E$_4$, −160° for ^{0}E, −55° for E$_1$, −50° for ^{2}E, and so on). The minimum-energy conformation is found for the E$_4$ (anti) and ^{0}E (syn) forms. The −*sc* rotamers having the anti orientation show H bonds of the exocyclic amino group with O5′ for the ^{3}E, E$_1$, ^{2}E, E$_3$, and ^{4}E envelope forms, which could justify the ^{3}E and ^{2}E puckering as the minimum energy conformations. The syn orientation induces the

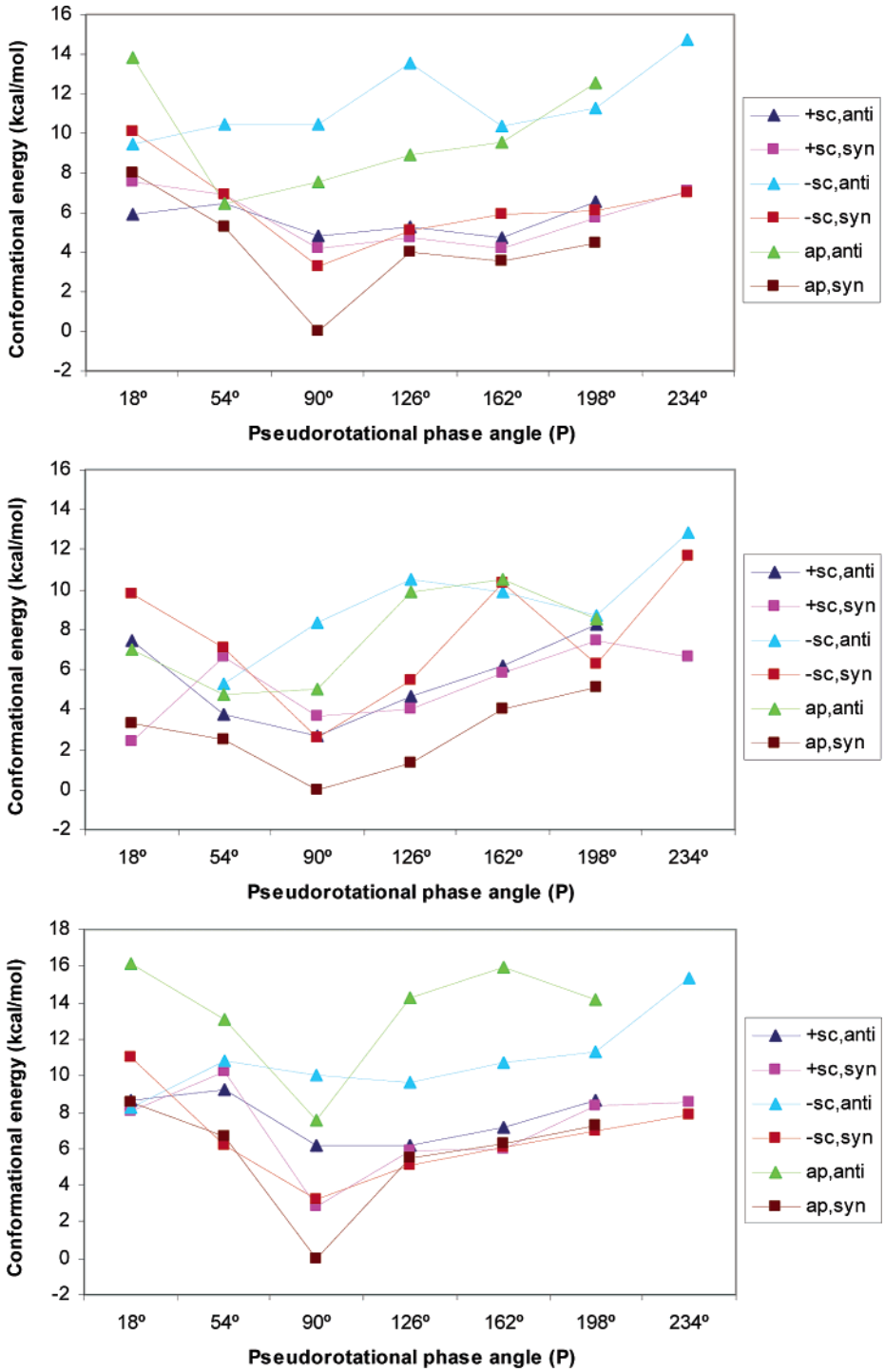

Figure 6. Conformational energy profiles in the gas phase for **10** (top), **11** (middle), and **12** (bottom) as a function of the C4′−C5′ and glycosidic bond torsion angles.

stabilization of the E_4, ^0E, and E_1 forms through the noncovalent interaction of the amino group with the pyrimidinic O4, whereas the ^2E form shows the interaction with O5′.

Overall, in the gas phase, the syn orientation involves energy profiles shifted downward in energy where the minimum energy structures are by 0.6−7.6 kcal mol^{-1} relative to the anti equivalent conformations.

For the isothiazolic derivative **11**, the energy profiles show some parallel trends, and additionally, we can observe that the endocyclic NH group exerts stabilizing effects. The *ap* and +*sc* rotamers present related conformational properties to the oxathiole, yielding minimal energy structures located at E_4 and ^0E. The isothiazolic NH group forms intramolecular H bonds with the neighboring O2′ (2.0−2.4 Å), thus stabilizing all conformations but ^2E and E_3, where such interaction should induce a highly strained structure. The absence of this additional bond could account for the high energy shown in the profiles for both conformers. Moreover, the unexpected stability for E_4 for the −*sc* anti rotamer is due to the striking H bond of the NH moiety with O5′, while the presence of this group drives the ring-puckering change $^3E \rightarrow E_3$ upon optimization.

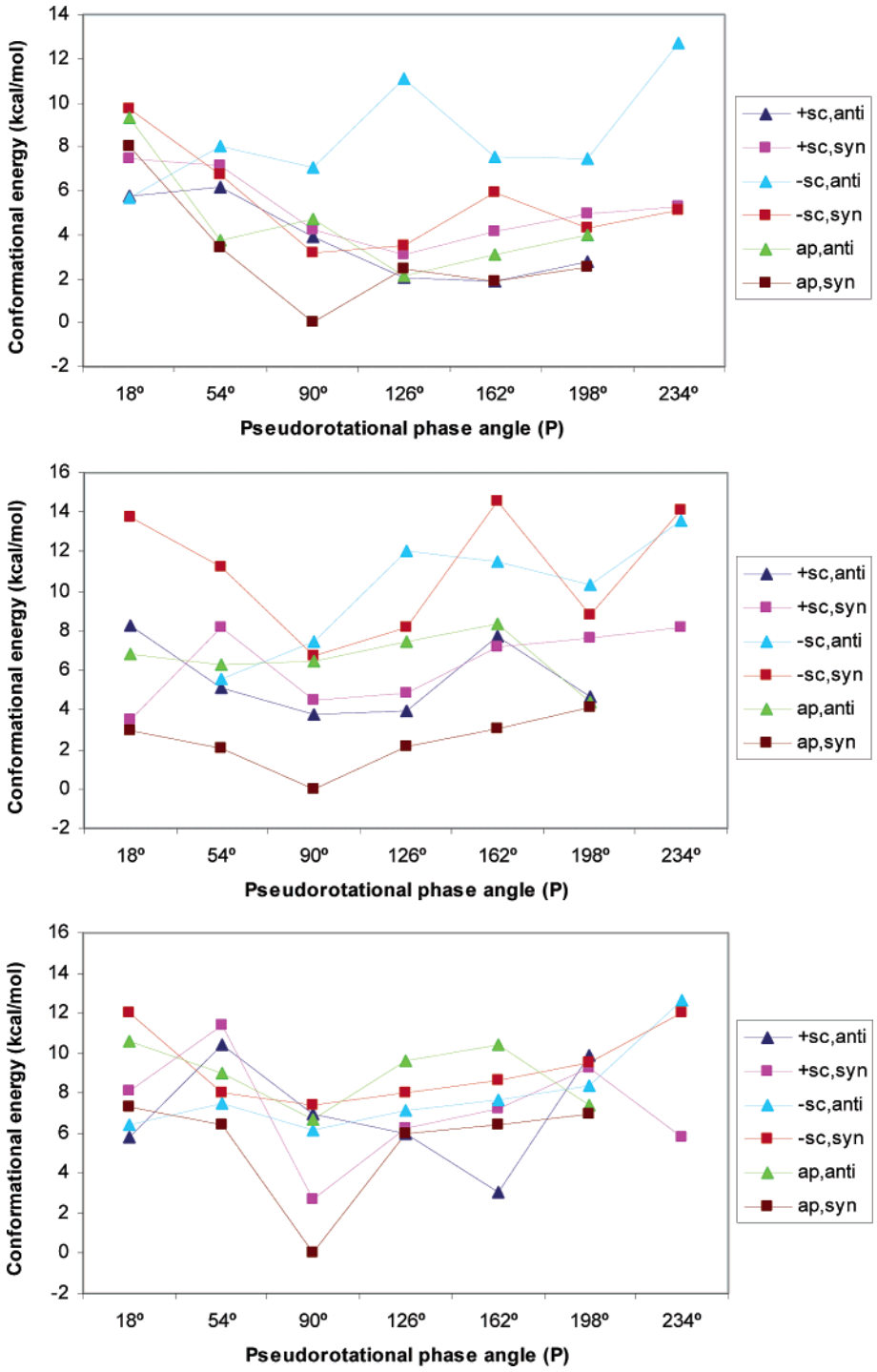

Figure 7. Conformational energy profiles in the aqueous phase for **10** (top), **11** (middle), and **12** (bottom) as a function of the C4′−C5′ and glycosidic bond torsion angles.

The methyl derivative **12** displays a qualitatively similar H-bonding pattern to that of the oxathiole structure. However, the alkyl substituent exerts steric effects which cannot be minimized via nitrogen pyramidalization because of strong repulsion between the lone pairs at N and the neighboring O2′. Predictably, this repulsion is particularly relevant for structures showing C1′−C2′−C3′−C4′ torsion angle (ν_2) values far from zero, such as for ^{2}E puckering. Indeed, the ^{0}E form presents the longest N···O2′ distance for every plausible rotamer and the lowest energy conformer. These results point to a higher ring rigidity enhanced by the alkyl substituent.

During optimizations of the ^{4}E envelope form for the *ap* and *+sc* anti conformers for the three derivatives, a spontaneous ring inversion afforded the E_4 geometry because of strong 1,3-diaxial interactions. A nearly planar ring ($\nu_m = 8-15°$) was observed for this envelope form for the other rotamers.

When electrostatic solvent effects are taken into account (Figure 7), qualitative parallel profiles are observed, except for the *ap* anti conformers for **10**. As we have noted above, a backbone torsion around the C2′−O2′ bond is detected for the southern region of the pseudorotational cycle because of a strong electrostatic repulsion between O2′ and the

Table 1. Optimizations at the DFT Level[a]

	label	starting structure[b]	P (ν_m) ($\epsilon = 4.0$)	P (ν_m) ($\epsilon = 78.4$)	relative energy (in kcal mol^{-1}) ($\epsilon = 4.0$)	relative energy (in kcal mol^{-1}) ($\epsilon = 78.4$)
10	**a**	^{0}E, *ap*, *syn*	80.0 (45.3)	81.1 (45.5)	0.00	0.00
	b	^{0}E, *ap*, *anti*	70.7 (50.0)	72.3 (48.9)	+6.59	+3.89
	c	^{2}E, +*sc*, *anti*	154.2 (38.7)	158.1 (39.1)	+3.25	+1.91
	d	^{2}E, −*sc*, *anti*	159.8 (39.3)	162.3 (39.9)	+8.32	+7.02
	e	^{3}E, +*sc*, *anti*	24.6 (37.9)	29.8 (37.2)	+5.49	+5.91
	f	E_4, +*sc*, *anti*	65.7 (35.4)	72.4 (47.5)	+4.24	+5.17
	g	E_4, *ap*, *anti*	45.2 (38.6)	50.3 (39.0)	+6.26	+8.30
11	**a**	^{0}E, *ap*, *syn*	83.3 (44.2)	84.2 (44.3)	0.00	0.00
	b	^{0}E, *ap*, *anti*	75.0 (48.6)	74.2 (47.5)	+5.07	+2.76
	c	^{2}E, +*sc*, *anti*	159.3 (38.1)	164.6 (38.4)	+1.80	+3.12
	d	^{2}E, −*sc*, *anti*	157.5 (39.7)	160.1 (40.0)	+10.26	+9.44
	e	^{3}E, +*sc*, *anti*	29.0 (37.2)	31.4 (36.9)	+7.38	+7.97
	f	E_4, +*sc*, *anti*	75.1 (45.6)	73.2 (46.0)	+2.32	+3.93
	g	E_4, *ap*, *anti*	60.7 (43.3)	62.9 (43.7)	+4.48	5.96
12	**a**	^{0}E, *ap*, *syn*	88.5 (42.8)	89.9 (43.5)	0.00	0.00
	b	^{0}E, *ap*, *anti*	79.3 (48.0)	80.8 (47.5)	+3.67	+2.89
	c	^{2}E, +*sc*, *anti*	163.0 (42.3)	164.9 (42.8)	+6.75	+8.23
	d	^{2}E, −*sc*, *anti*	166.2 (42.6)	168.0 (43.4)	+10.41	+10.68
	e	^{3}E, +*sc*, *anti*	59.4 (40.1)	60.3 (40.7)	+13.36	+11.94
	f	E_4, +*sc*, *anti*	81.3 (45.1)	80.5 (45.6)	+2.74	+4.18
	g	E_4, *ap*, *anti*	61.3 (43.3)	65.6 (40.6)	+11.88	+12.22

[a] Pseudorotational parameters P and ν_m (in deg) are also shown. [b] Constrained ab initio structure used as input.

endocyclic spiro oxygen, O2′ laying solvent-exposed, and hence stabilized by electrostatic solvation. This structural feature may explain the high stability in solution for E_1 and ^{2}E puckering modes relative to the most stable structure in the gas phase, E_4. For **11** and **12**, such electrostatic repulsion is absent. Quantitatively, the main difference between gas- and aqueous-phase profiles arises from the stabilization of the *ap* anti conformers because the distant O5′ and thymine carbonyl groups are not involved in intramolecular H bonding and are exposed to the outside, so they can be efficiently solvated by the polar medium, giving rise to strong conformer stabilization. In general, the syn rotamers are less affected.

3.3.3. DFT Calculations. Although a rough approximation, the analysis shown above provides a global overview of the conformational behavior of these compounds. It may be supposed that the RT-binding process for the inhibitor would involve a desolvation step and a conformational change from the most stable structure in solution to the conformation adopted in the complex. The previous results have suggested that the lowest-energy conformation in aqueous solution presents an ^{0}E form, *ap* rotation around C4′−C5′ bond, and syn orientation of the base. On the other hand, the docked study, as well as a prior MD simulation reported by Gago et al.,[16] suggests a different conformation upon binding: the 3′-spiro NH_2 group for an anti conformer may interact with the critical GluB138 amino acid better than a syn one; the 5′-TBDMS group may be easier accommodated on the presumed hydrophobic pocket (p51 subunit) for an *ap* rotamer than for other rotamers. In this way, the lowest-energy form found for *ap* anti isomers in the gas phase (i.e., low-dielectric medium) is an E_4 puckering for **10** and **11** and ^{0}E for **12**.

To obtain more reliable energy differences, we have performed unconstrained reoptimizations at the DFT level [B3LYP/6-31+G(2d,p)//B3LYP/6−31(d), see Computational Methods for details]. Besides these relevant conformers (*ap* syn ^{0}E, *ap* anti E_4, and *ap* anti ^{0}E), we have also included other representative conformations in our calculations. Thus, a +*sc* anti ^{2}E conformation was detected from a crystallographic analysis for the related structure TSAO-m^{3}T,[15] whereas ^{2}E and ^{3}E puckering modes, along with ^{0}E, have been reported from MD simulations for the same compound.[16]

The energy differences computed in a physiological environment ($\epsilon = 4.0$) and in aqueous solution ($\epsilon = 78.4$) are summarized in Table 1. Predictably, the lowest-energy conformer is a *ap* syn rotamer showing an ^{0}E envelope puckering, although the anti equivalent rotamer is only slightly higher in energy in aqueous solution. Interestingly, for the oxathiole derivative, the pseudorotational parameters calculated for the most stable geometry **10a** ($P = 81.1°$, $\nu_m = 45.5°$) are very close to those observed for the prototype TSAO-T ($P = 86°$, $\nu_m = 42°$) from NMR studies,[19a] and the relatively high stability of the +*sc* anti ^{2}E conformer **10c** (+1.91 kcal mol^{-1}) is consistent with previous X-ray crystallographic studies on TSAO-m^{3}T which identified this conformer.[15] These results give us confidence in the theoretical model applied.

The results also highlight the effects of the methyl group in **12** previously pointed out by the ab initio profiles. The optimization of initial structures where ν_2 (C1′−C2′−C3′−C4′ torsion angle) is far from zero drives to final structures close to the ^{0}E puckering mode. In fact, the full optimization of the ^{0}E constrained structures (**a** and **b**) for **12** lead to the lowest deviation from the pure ^{0}E mode. The energy values also indicate a lesser stability for those structures far from the ^{0}E form. In contrast, **10** and **11** show a higher flexibility, and conformers with P values ∼ 25° (corresponding to an ^{3}E envelope conformation) were obtained as stable structures.

4. DISCUSSION

The SAR results accumulated in recent years for TSAO derivatives have revealed severe structural requirements, suggesting that the binding site would not be flexible enough to easily accommodate the sugar substituents. In this sense, the critical role played by the 5′ substituent for activity is

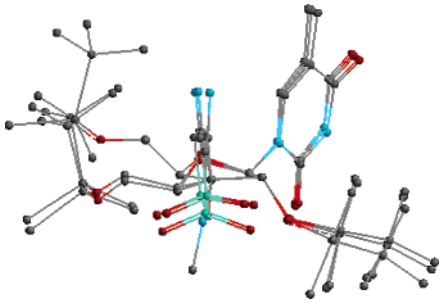

Figure 8. Superposition of the optimized structures **1**, **3**, and **7** showing the larger deviation of the 5′ group for **7**.

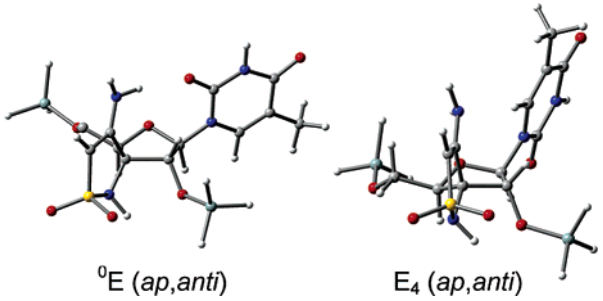

Figure 9. DFT-optimized structures for **11**: the lowest energy conformation in aqueous solution (**11a**, left) and presumed conformation in the macromolecular environment (**11g**, right).

Table 2. Energy Variation for the Proposed Conformational Change upon Binding

	conformational change	ΔE_{Desolv} (kcal mol^{-1})	ΔE_{Conf} (kcal mol^{-1})	ΔE_{TOTAL} (kcal mol^{-1})
10	a → g	4.66	6.26	10.92
11	a → g	7.17	4.48	11.65
12	a → b	2.48	3.67	6.15
	a → g		11.88	14.36

remarkable.[18c] The superposition of the sugar ring for the three structures **1**, **3**, and **7** shows a larger deviation for the 5′ substituent for **7** (Figure 8). So, it may be supposed that a restricted ring flexibility could avoid an efficient interaction with the protein and, hence, induce a lower inhibitory activity.

According to the results summarized in Figure 6, the lowest-energy conformation found in the gas phase for the *ap* anti rotamer for **10** and **11** is a E$_4$, while for **12**, it is an ^{0}E puckering. Therefore, the DFT-calculated energy penalties on passing from the lowest-energy conformation in solution to the these forms in the macromolecular phase (see Figure 9 for **11**) are 10.92, 11.65, and 6.15 kcal/mol for **10**, **11**, and **12** (Table 2), respectively, which cannot account for the inhibitory activity observed. However, a conformational change to the **g** puckering for **12** to achieve the stringent structural requirements in the binding site involves an energy of 11.88 kcal mol^{-1}, which increases the total energy penalty to 14.36 kcal mol^{-1}, higher than that for **10** and **11**, which could justify, at least partially, the ∼10-fold lesser inhibitory activity of the methylated derivatives as compared to that of the unsubstituted derivatives.

In addition to this conformational-based rationalization, the docking study suggests a binding mode where the endocyclic amino group in the 3′-spiro moiety would be mostly exposed to the solvent. Figure 10 displays the molecular surfaces of the compounds **1**, **3**, and **7**, colored in accordance with the electrostatic potential. These surfaces correspond to an isodensity value of 0.001 au, that is, the van der Waals surface approximately, a representation of particular interest to highlight the noncovalent interactions occurring at the molecular surface. These electrostatic potential maps show a negative region (orange) around the endocyclic spiro oxygen for **1** and a positive region (blue) due to the polar hydrogen of the endocyclic amino group for **3**. Both polar regions are able to interact with the polar solvent. In contrast, **7** presents an apolar region (green). In this way, additional electrostatic stabilization by the polar solvent can take place for the complex formed with the oxathiole and unmethylated aza derivatives.

5. CONCLUSIONS

The aza analogues of TSAO with diverse substitution on both *N*-3 and *N*-2″ positions present the same binding mode to the TSAO-T prototype, as determined by docking studies. This molecular model reveals that the endocyclic amino group is mostly exposed to the solvent. Hence, the fact that the methylated compounds exhibit a ∼10-fold lesser inhibitory activity against HIV-1 RT than that of the unsubstituted ATSAO derivatives may be related with a poorer stabilization by solvation of this group and, additionally, by conformational preferences induced by the substituent.

On the basis of the present conformational study, we have observed that, while the TSAO-T model and the unsubstituted ATSAO present similar conformational properties, the substituent on the nitrogen atom in the spiro moiety constrains the ring pucker to a narrow region of the pseudorotational cycle. This leads to a rather altered spatial disposition of the base and substituents of furanose: the 3″-spiro, 2′-*O*-, and mainly 5′-*O*-TBDMS groups. Because a very rigorous geometric requirement for the 5′ moiety has been recognized, it can be speculated that the suitable adaptation to the binding site may be hampered because of this enhanced conformational rigidity, in such a way that

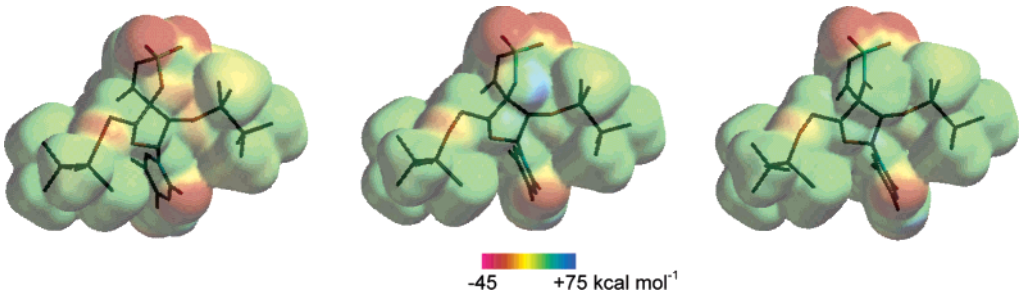

Figure 10. Molecular electrostatic potential maps (RHF/6-31G*) of **1** (left), **3** (middle), and **7** (right) computed at the van der Waals surface (0.001 au).

this substituent cannot be optimally accommodated without a loss of affinity. The computed change in energy on passing from the lowest-energy conformation in solution to that probably adopted in the complex reveals a higher energy penalty for the methyl derivative, whereas the TSAO-T and the unsubstituted aza analogue afford similar values. Hence, the reduced activity might be related to subtle conformational preferences and electrostatic effects with the bulk water.

ACKNOWLEDGMENT

J.L.M. and E.S. thank Profs. Paloma Ballesteros (UNED, Spain) and Sebastián Cerdán (IIB, Madrid, Spain) for continuous support and encouragement. E.S. thanks Gobierno de La Rioja for a postdoctoral fellowship. D.P., A.N., and C.T. thank the Conseil Régional de Picardie and the Ministère Français de la Recherche for supporting this work.

Supporting Information Available: Concepts on sugar pucker, a comparison between the conformational analysis (molecular mechanics) for **1** and **10**, and docking parameters. This material is available free of charge via the Internet at http://pubs.acs.org.

REFERENCES AND NOTES

(1) Wang, J.; Smerdon, S. J.; Jager, J.; Kohlstaedt, L. A.; Rice, P. A.; Friedman, J. M. Structural Basis of Asymmetry in the Human Immunodeficiency Virus Type 1 Reverse Transcriptase Heterodimer. *Proc. Natl. Acad. Sci. U.S.A.* **1994**, *91*, 7242−7246.

(2) Nanni, R. G.; Ding, J.; Jacobo-Molina, A.; Hughes, S. H.; Arnold, E. Review of HIV−I Reverse Transcriptase 3-Dimensional Structure: Implication for Drug Design. *Perspect. Drug Discovery Des.* **1993**, *1*, 129−150.

(3) Harris, D.; Lee, R.; Misra, H. S.; Pandey, P. K.; Pandey, V. N. The p51 Subunit of Human Immunodeficiency Virus Type 1 Reverse Transcriptase Is Essential in Loading the p66 Subunit on the Template Primer. *Biochemistry* **1998**, *37*, 5903−5908.

(4) Restle, T.; Muller, B.; Godoy, R. S. RNase H Activity of HIV Reverse Transcriptases Is Confined Exclusively to the Dimeric Forms. *FEBS Lett.* **1992**, *300*, 97−100.

(5) Restle, T.; Muller, B.; Godoy, R. S. Dimerization of Human Immunodeficiency Virus Type 1 Reverse Transcriptase: A Target for Chemotherapeutic Intervention. *J. Biol. Chem.* **1990**, *265*, 8986−8988.

(6) (a) Balzarini, J.; Pérez-Pérez, M. J.; San-Félix, A.; Schols, D.; Perno, C. F.; Vandamme, A. M.; Camarasa, M. J.; De Clercq, E. 2′,5′-Bis-O-(*tert*-butyldimethylsilyl)-3′-spiro-5″-(4″-amino-1″,2″-oxathiole-2″,2-dioxide) Pyrimidine (TSAO) Nucleoside Analogues: Highly Selective Inhibitors of Human Immunodeficiency Virus Type 1 That Are Targeted at the Viral Reverse Transcriptase. *Proc. Natl. Acad. Sci. U.S.A.* **1992**, *89*, 4392−4396. (b) Balzarini, J.; Pérez-Pérez, M.-J.; San-Félix, A.; Velázquez, S.; Camarasa, M. J.; De Clercq, E. [2′,5′-Bis-O-(*tert*-butyldimethylsilyl)]-3′-spiro-5″-(4″-amino-1″,2″-oxathiole-2″,2″-dioxide) (TSAO) Derivarives of Purine and Pyrimidine Nucleosides as Potent and Selective Inhibitors of Human Immunodeficiency Virus Type 1. *Antimicrob. Agents Chemother.* **1992**, *36*, 1073−1080.

(7) Sluis-Cremer, N.; Arion, D.; Parniak, M. A. Destabilization of the HIV-1 Reverse Transcriptase Dimer upon Interaction with N-Acyl Hydrazone Inhibitors. *Mol. Pharmacol.* **2002**, *62*, 398−405.

(8) (a) Tachedjian, G.; Goff, S. P. The Effect of NNRTIs on HIV Reverse Transcriptase Dimerization. *Curr. Opin. Invest. Drugs* **2003**, *4*, 966−973. (b) Tachedjian, G.; Orlova, M.; Sarafianos, S. G.; Arnold, E.; Goff, S. P. Nonnucleoside Reverse Transcriptase Inhibitors Are Chemical Enhancers of Dimerization of the HIV Type 1 Reverse Transcriptase. *Proc. Natl. Acad. Sci. U.S.A.* **2001**, *98*, 7188−7193.

(9) Camarasa, M.-J.; Pérez-Pérez, M.-J.; San-Félix, A.; Balzarini, J.; De Clercq, E. 3′-Spiro Nucleosides, a New Class of Specific Human Immunodeficiency Virus Type Inhibitors: Synthesis and Antiviral Activity of [2′,5′-Bis-*O*-(*tert*-butyldimethylsilyl)-β-D-ribofuranose]-3′-spiro-5″-[4″-amino-1″,2″-oxathiole-2″,2″-dioxide] (TSAO) Pyrimidine Nucleosides. *J. Med. Chem.* **1992**, *35*, 2721−2727.

(10) Balzarini, J.; Perez-Perez, M.-J.; San-Felix, A.; Camarasa, M.-J.; Bathurst, I. C.; Barr, P. J.; DeClercq, E. Kinetics of Inhibition of Human Immunodeficiency Virus Type 1 (HIV-1) Reverse Transcriptase by the Novel HIV-1 Specific Nucleoside Analogue 2′,5′-Bis-O-(*tert*-butyldimethylsilyl)-3′-spiro-5″-(4″-amino-1″,2″-oxathiole-2″,2″-dioxide) thymine (TSAO-T). *J. Biol. Chem.* **1992**, *267*, 11831−11838.

(11) (a) Balzarini, J.; Velazquez, S.; San-Felix, A.; Karlsson, A.; Perez-Perez, M. J.; Camarasa, M. J.; De Clercq, E. The HIV-l-specific TSAO-Purine Analogues Show a Resistance Spectrum That Is Different from That of the HIV-l-specific Non-nucleoside Analogues. *Mol. Pharmacol.* **1993**, *43*, 109−114. (b) Jonckheere, H.; Taymans, J. M.; Balzarini, J.; Velázquez, S.; Camarasa, M. J.; Desmyter, J.; De Clercq, E.; Anne, J. Resistance of HIV-1 Reverse Transcriptase against [2′, 5′-Bis-O-(*tert*-butyldimethylsilyl)-3′spiro-5″-(4″-amino-1″,2″-oxathiole-2″,2″-dioxide)] (TSAO) Derivatives Is Determined by the Mutation Glu138 → Lys on the p51 Subunit. *J. Biol. Chem.* **1994**, *69*, 25255−25258.

(12) Boyer, P. L.; Ding, J.; Arnold, E.; Hughes, S. H. Subunit Specificity of Mutations that Confer Resistance to Nonnucleoside Inhibitors in Human Immunodeficiency Virus Type 1 Reverse Transcriptase. *Antimicrob. Agents Chemother.* **1994**, *38*, 1909−1914.

(13) Arion, D.; Fletcher, R. S.; Borkow, G.; Camarasa, M. J.; Balzarini, J.; Dmitrienko, G. I.; Parniak, M. A. Differences in the Inhibition of Human Immunodeficiency Virus Type 1 Reverse Transcriptase DNA Polymerase Activity by Analogues of Nevirapine and [2′,5′-Bis-O-(tertbutyldimethylsilyl)-3′-spiro-5″-(4″-amino-1″,2″-oxathiole-2″,2″-dioxide] (TSAO). *Mol. Pharmacol.* **1996**, *50*, 1057−1064.

(14) Pandey, P. K.; Kaushik, N.; Talele, T. T.; Yadav, P. N. S.; Pandey, V. N. The β7-β8 Loop of the p51 Subunit in the Heterodimeric (p66/p51) Human Immunodeficiency Virus Type 1 Reverse Transcriptase is Essential for the Catalytic Function of the p66 Subunit. *Biochemistry* **2001**, *40*, 9505−9512.

(15) Sluis-Cremer, N.; Dmitrienko, G. I.; Balzarini, J.; Camarasa, M. J.; Parniak, M. A. Human Immunodeficiency Virus Type 1 Reverse Transcriptase Dimer Destabilization by 1-[Spiro[4″-amino-2″,2″-dioxo-1″,2″-oxathiole-5″,3′-[2′,5′-bis-O−(*tert*-butyldimethylsilyl)-β-D-ribofuranosyl]]]-3-ethylthymine. *Biochemistry* **2000**, *39*, 1427−1433.

(16) Rodríguez-Barrios, F.; Pérez, C.; Lobatón, E.; Velázquez, S.; Chamorro, C.; San-Félix, A.; Pérez-Pérez, M. J.; Camarasa, M. J.; Pelemans, H.; Balzarini, J.; Gago, F. Identification of a Putative Binding Site for [2′,5′-Bis-O-(*tert*-butyldimethylsilyl)-β-D-ribofuranosyl]-3′-spiro-5″-(4″-amino-1″,2″-oxathiole-2″,2″-dioxide)thymine (TSAO) Derivatives at the p51−p66 Interface of HIV-1 Reverse Transcriptase. *J. Med. Chem.* **2001**, *44*, 1853−1865.

(17) Camarasa, M. J.; Pérez-Pérez, M. J.; Velázquez, S.; San-Félix, A.; Alvarez, R.; Ingate, S.; Jimeno, M. L.; De Clercq, E.; Balzarini, J. An Overview of TSAO-T Derivatives, a "Peculiar" Class of HIV-1 Specific RT Inhibitors. In *Antiinfectives. Recent Advances in Chemistry and Structure−Activity Relationships*. Bentley, P. H., O'Hanlon, P. J., Eds.; The Royal Society of Chemistry: Letchworth, U. K., 1997; Chapter 18, pp 259−268.

(18) (a) Pérez-Pérez, M.-J.; San-Félix, A.; Balzarini, J.; De Clercq, E.; Camarasa, M.-J. TSAO-Analogues. Stereospecific Synthesis and Anti-HIV-1 Activity of 1-[2′,5′-Bis-*O*-(tertbutyldimethylsilyl)-(β-D-ribofuranosyl]-3′-spiro-5″-(4″-amino-1″,2″-oxathiole-2″,2″-dioxide)pyrimidine and Pyrimidine Modified Nucleosides. *J. Med. Chem.* **1992**, *35*, 2988−2995. (b) Ingate, S.; Pérez-Pérez, M. J.; De Clercq, E.; Balzarini, J.; Camarasa, M. J. Synthesis and Anti-HIV-1 Activity of Novel TSAO-T Derivatives Modified at the 2′- and 5′-Positions of the Sugar Moiety. *Antiviral Res.* **1995**, *27*, 281−299. (c) Chamorro, C.; Pérez-Pérez, M. J.; Rodríguez-Barrios, F.; Gago, F.; De Clercq, E.; Balzarini, J.; San-Félix, A.; Camarasa, M. J. Exploiting the Role of the 5′-Position of TSAO-T. Synthesis and Anti-HIV Evaluation of Novel TSAO-T Derivatives. *Antiviral Res.* **2001**, *50*, 207−222.

(19) (a) Alvarez, R.; Jimeno, M. L.; Gago, F.; Balzarini, J.; Perez-Perez, M. J.; Camarasa, M. J. Novel 3′-Spiro Nucleoside Analogues of TSAO-T. Part II. A Comparative Study based on NMR Conformational Analysis in Solution and Theoretical Calculations. *Antiviral Chem. Chemother.* **1998**, *9*, 333−340. (b) Lobatón, E.; Rodríguez-Barrios, F.; Gago, F.; Pérez-Pérez, M. J.; De Clercq, E.; Balzarini, J.; Camarasa, M. J.; Velázquez, S. Synthesis of 3″-Substituted TSAO Derivatives with Anti-HIV-1 and Anti-HIV-2 Activity through an Efficient Palladium-Catalyzed Crosscoupling Approach. *J. Med. Chem.* **2002**, *45*, 3934−3945.

(20) (a) Velázquez, S.; San-Félix, A.; Pérez-Pérez, M. J.; Balzarini, J.; De Clercq, E.; Camarasa, M. J. TSAO Analogues. 3. Synthesis and Anti-HIV-1 Activity of 2′,5′-Bis-O-(*tert*-butyldimethylsilyl)-β-D-ribofuranosyl-3′-spiro-5″-(4″-amino-1″,2″-oxathiole-2″,2″-dioxide) Purine and Purine-Modified Nucleosides. *J. Med. Chem.* **1993**, *36*, 3230−3239. (b) San-Félix, A.; Velázquez, S.; Pérez-Pérez, M. J.; Balzarini, J.; De Clercq, E.; Camarasa, M. J. Novel Series of TSAO-T Derivatives. Synthesis and Anti-HIV-1 Activity of 4-, 5-, and 6-Substituted Pyrimidine Analogues. *J. Med. Chem.* **1994**, *37*, 453−460. (c) Bonache, M. C.; Chamorro, C.; Velázquez, S.; De Clercq, E.; Balzarini, J.; Rodríguez-Barrios, F.; Gago, F.; Camarasa, M. J.; San-Félix, A.

Improving the Antiviral Efficacy and Selectivity of HIV-1 Reverse Transcriptase Inhibitor TSAO-T by the Introduction of Functional Groups at the N-3 Position. *J. Med. Chem.* **2005**, *48*, 6653−6660.
(21) Nguyen Van Nhien, A.; Tomassi, C.; Len, C.; Marco-Contelles, J.; Balzarini, J.; Pannecouque, C.; De Clercq, E.; Postel, D. First Synthesis and Evaluation of the Inhibitory Effects of Aza Analogues of TSAO on HIV-1 Replication. *J. Med. Chem.* **2005**, *48*, 4276−4284.
(22) Morris, G. M.; Goodsell, D. S.; Huey, R.; Hart, W. E.; Halliday, S.; Belew, R.; Olson, A. J. *AutoDock: Automated Docking of Flexible Ligands to Receptors*, version 3.05; The Scripps Research Institute: La Jolla, CA, 2000.
(23) Hsiou, Y.; Ding, J.; Das, K.; Clark, A. D., Jr.; Hughes, S. H.; Arnold, E. Structure of Unliganded HIV-1 Reverse Transcriptase at 2.7 Å Resolution: Implications of Conformational Changes for Polymerization and Inhibition Mechanisms. *Structure* **1996**, *4*, 853−860.
(24) Rodgers, D. W.; Gamblin, S. J.; Harris, B. A.; Ray, S.; Culp, J. S.; Hellmig, B.; Woolf, D. J.; Debouck, C.; Harrison, S. C. The Structure of Unliganded Reverse Transcriptase from the Human Immunodeficiency Virus Type 1. *Proc. Natl. Acad. Sci. U.S.A.* **1995**, *92*, 1222−1226.
(25) Hsiou, Y.; Das, K.; Ding, J.; Clark, A. D., Jr.; Kleim, J. P.; Rosner, M.; Winkler, I.; Riess, G.; Hughes, S. H.; Arnold, E. Structures of Tyr188Leu Mutant and Wild-Type HIV-1 Reverse Transcriptase Complexed with the Non-nucleoside Inhibitor hby 097: Inhibitor Flexibility Is a Useful Design Feature for Reducing Drug Resistanse. *J. Mol. Biol.* **1998**, *284*, 313−323.
(26) Ren, J.; Diprose, J.; Warren, J.; Esnouf, R.; Bird, L. E.; Ikemizu, S.; Slater, M.; Milton, J.; Balzarini, J.; Stuart, D. I.; Stammers, D. K. Phenyl Ethylthiazolylthiourea (PETT) Non-nucleoside Inhibitors of HIV-1 and HIV-2 Reverse Transcriptase. *J. Biol. Chem.* **2000**, *275*, 5633−5639.
(27) Ding, J.; Das, K.; Tantillo, C.; Zhang, W.; Clark, A. D., Jr.; Jessen, S.; Lu, X.; Hsiou, Y.; Jacobo-Molina, A.; Andries, K.; Pauwels, R.; Moereels, H.; Koymans, L.; Janssen, P. A. J.; Smith, R.; Koepke, M. K.; Michejda, C.; Hughes, S. H.; Arnold, E. Structure of HIV-1 Reverse Transcriptase in a Complex with the Nonnucleoside Inhibitor α-APA R 95845 at 2.8 Å Resolution. *Structure* **1995**, *3*, 365−379.
(28) Das, K.; Clark, A. D., Jr.; Lewi, P.; Heeres, J.; Dejonge, M.; Koymans, L.; Vinkers, H.; Daeyaert, F.; Ludovici, D. W.; Kukla, M. J.; Decorte, B.; Kavash, R. W.; Ho, C. Y.; Ye, H.; Lichtenstein, M.; Andries, K.; Pauwles, R.; Debethune, M.-P.; Boyer, P. L.; Clark, P.; Hughes, S. H.; Janssen, P. A.; Arnold, E. Roles of Conformational and Positional Adaptability in Structure-based Design of TMC125−R165335 (Etravirine) and Related Non-nucleoside Reverse Transcriptase Inhibitors that are Highly Potent and Effective Against Wild-Type and Drug-Resistant HIV-1 Variants. *J. Med. Chem.* **2004**, *47*, 2550−2560.
(29) Wang, J.; Smerdon, S. J.; Jager, J.; Kohlstaedt, L. A.; Rice, P. A.; Friedman, J. M.; Steitz, T. A. Structural Basis of Asymmetry in the Human Immunodeficiency Virus Type 1 Reverse Transcriptase Heterodimer. *Proc. Natl. Acad. Sci. U.S.A.* **1994**, *91*, 7242−7246.
(30) AutoDock Parameters. http://www.scripps.edu/pub/olson-web/doc/autodock/parameters.html (accessed Aug 2005).
(31) Frisch, M. J.; Trucks, G. W.; Schlegel, H. B.; Scuseria, G. E.; Robb, M. A.; Cheeseman, J. R.; Zakrzewski, V. G.; Montgomery, J. A., Jr.; Stratmann, R. E.; Burant, J. C.; Dapprich, S.; Millam, J. M.; Daniels, A. D.; Kudin, K. N.; Strain, M. C.; Farkas, O.; Tomasi, J.; Barone, V.; Cossi, M.; Cammi, R.; Mennucci, B.; Pomelli, C.; Adamo, C.; Clifford, S.; Ochterski, J.; Petersson, G. A.; Ayala, P. Y.; Cui, Q.; Morokuma, K.; Malick, D. K.; Rabuck, A. D.; Raghavachari, K.; Foresman, J. B.; Cioslowski, J.; Ortiz, J. V.; Stefanov, B. B.; Liu, G.; Liashenko, A.; Piskorz, P.; Komaromi, I.; Gomperts, R.; Martin, R. L.; Fox, D. J.; Keith, T.; Al-Laham, M. A.; Peng, C. Y.; Nanayakkara, A.; Gonzalez, C.; Challacombe, M.; Gill, P. M. W.; Johnson, B. G.; Chen, W.; Wong, M. W.; Andres, J. L.; Head-Gordon, M.; Replogle, E. S.; Pople, J. A. *Gaussian 98*, revision A.11.2; Gaussian, Inc.: Pittsburgh, PA, 2001.
(32) Bayly, C. I.; Cieplak, P.; Cornell, W. D.; Kollman, P. A. A Well-Behaved Electrostatic Potential Based Method Using Charge Restraints for Deriving Atomic Charges: The RESP Model. *J. Phys. Chem.* **1993**, *97*, 10269−10280.
(33) Goodford, P. J. A Computational Procedure for Determining Energetically Favorable Binding Sites on Biologically Important Macromolecules. *J. Med. Chem.* **1985**, *28*, 849−857.
(34) *GRID*, version 22b; Molecular Discovery Ltd.: London, United Kingdom. http://www.moldiscovery.com (accessed May 2005).
(35) *PC Spartan. Pro*, version 1.0.5; Wavefunction, Inc.: Irvine, CA, 2000.
(36) Chang, G.; Guida, W. C.; Still, W. C. An Internal Coordinate Monte Carlo Method for Searching Conformational Space. *J. Am. Chem. Soc.* **1989**, *111*, 4379−4386.
(37) Halgren, T. A. The Merck Force Field. *J. Comput. Chem.* **1996**, *17*, 490−519.
(38) Frisch, M. J.; Trucks, G. W.; Schlegel, H. B.; Scuseria, G. E.; Robb, M. A.; Cheeseman, J. R.; Montgomery, J. A.; Vreven, T.; Kudin, K. N.; Burant, J. C.; Millam, J. M.; Iyengar, S. S.; Tomasi, J.; Barone, V.; Mennucci, B.; Cossi, M.; Scalmani, G.; Rega, N.; Petersson, G. A.; Nakatsuji, H.; Hada, M.; Ehara, M.; Toyota, K.; Fukuda, R.; Hasegawa, J.; Ishida, M.; Nakajima, T.; Honda, Y.; Kitao, O.; Nakai, H.; Klene, M.; Li, X.; Knox, J. E.; Hratchian, H. P.; Cross, J. B.; Adamo, C.; Jaramillo, J.; Gomperts, R.; Stratmann, R. E.; Yazyev, O.; Austin, A. J.; Cammi, R.; Pomelli, C.; Ochterski, J. W.; Ayala, P. Y.; Morokuma, K.; Voth, G. A.; Salvador, P.; Dannenberg, J. J.; Zakrzewski, V. G.; Dapprich, S.; Daniels, A. D.; Strain, M. C.; Farkas, O.; Malick, D. K.; Rabuck, A. D.; Raghavachari, K.; Foresman, J. B.; Ortiz, J. V.; Cui, Q.; Baboul, A. G.; Clifford, S.; Cioslowski, J.; Stefanov, B. B.; Liu, G.; Liashenko, A.: Piskorz, P.; Komaromi, L.; Martin, R. L.; Fox, D. J.; Keith, T.; Al-Laham, M. A.; Peng, C. Y.; Nanayakkara, A.; Challacombe, M. P.; Gill, M. W.; Johnson, B. G.; Chen, W.; Wong, M. W.; González, C.; Pople, J. A. *Gaussian 03*, revision B.03; Gaussian, Inc.: Pittsburgh, PA, 2003.
(39) Church, T. J.; Carmichael, I.; Serianni, A. S. $^{13}C-^{1}H$ and $^{13}C-^{13}C$ Spin-Coupling Constants in Methyl β-D-Ribofuranoside and Methyl 2-Deoxy-β-D-erythro-pentofuranoside: Correlation with Molecular Structure and Conformation. *J. Am. Chem. Soc.* **1997**, *119*, 8946−8964.
(40) (a) Lee, C.; Yang, W.; Parr, R. Development of the Colle-Salvetti Correlation-Energy Formula into a Functional of the Electron Density. *Phys. Rev. B* **1988**, *37*, 785−789. (b) Becke, A. Density-Functional Thermochemistry. III. The Role of Exact Exchange. *J. Chem. Phys.* **1993**, *98*, 5648−5652.
(41) (a) Barone, V.; Cossi, M. Quantum Calculation of Molecular Energies and Energy Gradients in Solution by a Conductor Solvent Model. *J. Phys. Chem. A* **1998**, *102*, 1995−2001. (b) Cossi, M.; Rega, N.; Scalmani, G.; Barone, V. Energies, Structures, and Electronic Properties of Molecules in Solution with the C-PCM Solvation Model. *J. Comput. Chem.* **2003**, *24*, 669−681.
(42) Gordon, M. T.; Lowary, T. L.; Hadad, C. M. Probing Furanose Ring Conformation by Gas-Phase Computational Methods: Energy Profile and Structural Parameters in Methyl β-D-Arabinofuranoside as a Function of Ring Conformation. *J. Org. Chem.* **2000**, *65*, 4954−4963.
(43) Zhou, Z.; Madrid, M.; Madura, J. D. Docking of Non-nucleoside Inhibitors: Neotripterifordin and Its Derivatives to HIV-1 Reverse Transcriptase. *Proteins* **2002**, *49*, 529−542.
(44) *Molecular Interaction Fields: Applications in Drug Discovery and ADME Prediction*, 1st ed.; Cruciani, G., Ed.; Wiley-VCH: Weinheim, Germany, 2005.
(45) Altona, C.; Sundaralingam, M. Conformational Analysis of the Sugar Ring in Nucleosides and Nucleotides. A New Description Using the Concept of Pseudorotation. *J. Am. Chem. Soc.* **1972**, *94*, 8205−8212.
(46) Westhof, E.; Sundaralingam, M. A Method for the Analysis of Puckering Disorder in Five-Membered Rings: The Relative Mobilities of Furanose and Proline Rings and Their Effects on Polynucleotide and Polypeptide Backbone Flexibility. *J. Am. Chem. Soc.* **1983**, *105*, 970−976.
(47) Liébecq, C. *Biochemical Nomenclature and Related Documents − A Compendium*, 2nd ed.; Portland Press on behalf of IUBMB: London, 1992.
(48) Alvarez, R.; Jimeno, M. L.; Gago, F.; Balzarini, J.; Pérez-Pérez, M. J.; Camarasa, M. J. Novel 3′-Spiro Nucleoside Analogues of TSAO-T. Part II. A Comparative Study Based on NMR Conformational Analysis in Solution and Theoretical Calculations. *Antiviral Chem. Chemother.* **1998**, *9*, 333−340.
(49) We have observed a minor anomeric effect along these calculations. The conformers showing quasi-axial orientation of the glycosidic bond, where such an effect could be more significant, have shown similar C1−O4 bond lengths to those of the quasi-equatorial orientation forms. Furthermore, NBO analyses have revealed only minor variations in the electron delocalizations due to the $n_{O4} \rightarrow \sigma_{C1-N1}^*$ interactions.

CI0600410